Synthetic spatial coherence function for optical tomography and profilometry: influence of the observation condition

Zhihui Duan[*a], Hirokazu Kozaki[a], Yoko Miyamoto[a], Joseph Rosen[b], and Mitsuo Takeda[a]

[a]The Univ. of Electro-Communications, Dept. of Information and Communication Engineering, 1-5-1 Chofugaoka, Chofu, Tokyo, 182-8585, Japan;
[b]Ben-Gurion Univ. of the Negev, Dept. of Electrical and Computer Engineering, P.O. Box 653, Beer-Sheva 84105, Israel

ABSTRACT

We address the basic issue of the observation condition in a synthetic coherence function applied to optical tomography and profilometry, which has not been made clear in previous papers. We present a more general theory for interference fringe formation for spatial coherence control with a synthetic source. The generalized theory predicts the existence of the observation condition that can make the measurement insensitive to the tilt of the object, which will open the new possibility of measuring objects with rough surfaces. We present experimental results that quantitatively verify the validity of the principle and the prediction.

Keywords: Spatial coherence, observation condition, coherence control, profilometry, optical tomography

1. INTRODUCTION

The existing techniques of OCT and low coherence interferometry are all based on the temporal coherence characteristic of broadband source[1-2]. Therefore, they suffer from a dispersion problem in many practical applications such as biological applications, where dispersion of the object and/or the light propagation medium is unavoidable. Rosen and Takeda[3] have proposed an alternative principle of optical tomography and profilometry based on spatial, rather than temporal, coherence. Instead of a point source with a broad spectrum, an extended source with a narrow spectrum was used in this technique. A desired longitudinal coherence function was synthesized by controlling the spatial structure of an extended quasi-monochromatic spatially incoherent light source. Besides solving the dispersion problem, the proposed technique enabled longitudinal coherence scan and phase shift without mechanical movement of a mirror for changing the optical path difference. Several papers have been published on spatial coherence control[4-10], but in most of the papers[6-7] the discussions were centered on how the coherence function is related to the distance and the tilt between the object and the reference mirror. From the theory of fringe localization, one can expect that even for an identical optical system with the same distance and tilt between the object and the reference mirror, the observed fringe contrast will be significantly different depending on the location where the observation lens is focused.
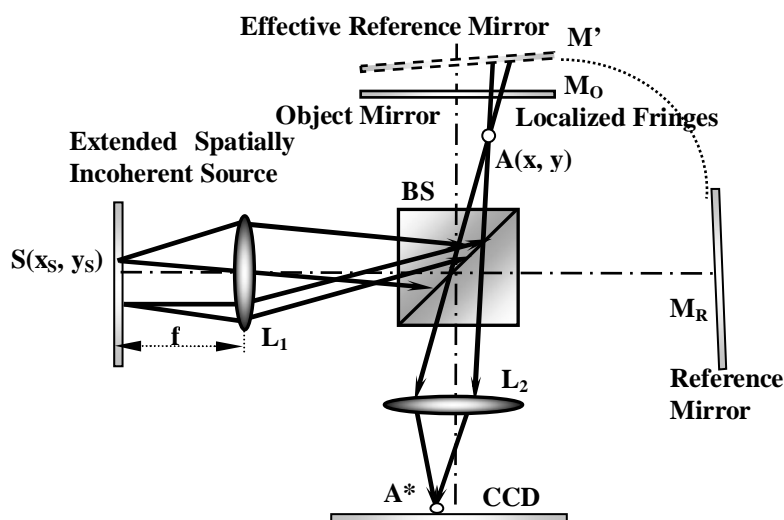

Fig.1. Interferometric system for controlling and measuring spatial coherence function.

The purpose of this paper is to address this basic issue of focusing condition, and to present a generalized theory for interference fringe formation with a synthetic source for spatial coherence control. A new formula obtained from the

generalized theory predicts the possibility of measuring an object with rough surfaces, which are demonstrated by experiment.

2. PRINCIPLE

Although the models in the previous papers[3-8] were able to explain the basic principle of spatial coherence control, they did not give a clear account of the role played by the imaging lens that actually determines the condition of observation. Here we introduce yet another model of fringe formation to clarify the role of the imaging lens. As shown in Fig. 1, a Michelson interferometer is illuminated by an extended quasi-monochromatic spatially incoherent light source S, which is located in the front focal plane of lens L_1. Light emitted from a point source on S is collimated by lens L_1 and split into two beams by prism beam splitter BS. The two beams are recombined by the beam splitter after being reflected by object mirror M_O and reference mirror M_R. The interference fringes generated on the CCD image sensor are the result of combination of images of the two optical field distributions, i.e., the optical field distributions from object mirror M_O and reference mirror M_R. Lens L_2 is focused on an arbitrary observation point A near or on the surface of object mirror M_O and forms its image onto the CCD image sensor. Seen from the side of CCD image sensor through the beam splitter BS, the virtual image of reference mirror M_R serves as an effective reference mirror M'_R located immediately behind the object mirror.
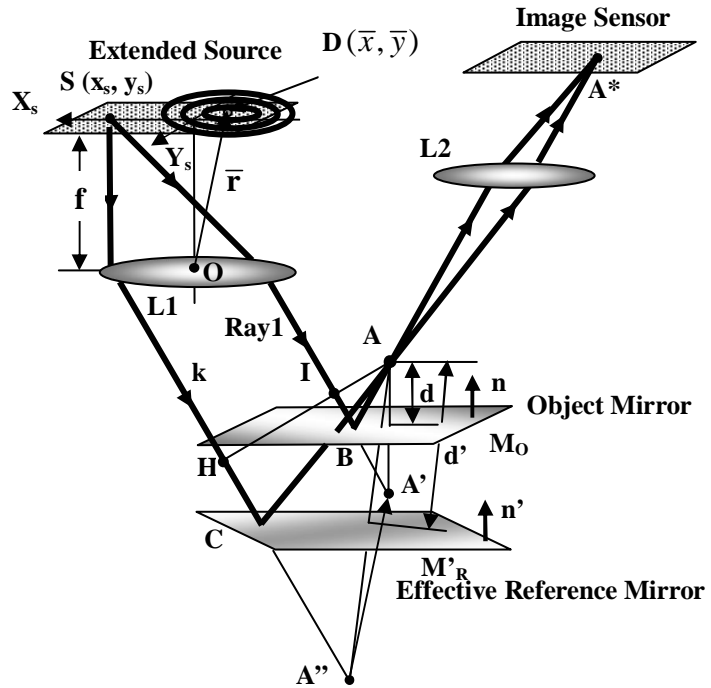

Fig.2. Formation of fringes at an arbitrary observation point.

Now let us generalize our theory allowing the observation point A to be located at an arbitrary point in the interferometer. Fig.2 shows how the fringes are formed on the CCD image sensor by the interferometer shown in Fig.1. For the convenience of visualization of ray paths, the optical axes of lens L1 and L2 are translated. Light emitted from a point source at (x_S, y_S) on the extended source S (placed in the front focal plane of lens L_1) is collimated by lens L_1 whose optical axis is in the direction of unit vector $\mathbf{n_0} = (0, 0, 1)$. Suppose that the imaging lens L_2 (which is focused on a point A at lateral position (x, y) and at distances d and d' from object mirror M_O and effective reference mirror M'_R, respectively) forms the image of the point A onto the CCD image sensor at point A*. Let the mirror images of point A with reference to object mirror M_O and effective reference mirror M'_R be A' and A", respectively. One of the rays in the collimated beam, directed to point A' and denoted by Ray1, is reflected by object mirror M_O at point B and reaches the observation point A. We also note another collimated ray, Ray2, from the same point source, which is directed to point A". This ray is reflected at point C by the effective (virtual) reference mirror M'_R, and then meets Ray1 at point A to generate interference fringes. Because lens L2 images point A onto the image sensor, the intensity recorded by the image sensor at point A* is the result of the interference between Ray1 and Ray2 at the observation point A. The phase difference between these two rays is given by

$$\delta(x_S, y_S; x, y) = k(\overline{\text{HCA}} - \overline{\text{IBA}}) = k(\overline{\text{HCA"}} - \overline{\text{IBA'}})$$

$$= \mathbf{k} \cdot (\overrightarrow{\text{AA"}} - \overrightarrow{\text{AA'}}) = \mathbf{k} \cdot (-2d'\mathbf{n'} + 2d\mathbf{n}),$$

(1)

where I and H are the points at which the normal line from point A crosses with Ray1 and Ray2,

$$\mathbf{k} \approx \frac{2\pi}{\lambda}\left(-\frac{x_S}{f}, -\frac{y_S}{f}, -(1-\frac{x_S^2+y_S^2}{2f^2})\right) \quad \text{under paraxial approximation, and} \quad \mathbf{n} = (\alpha_X, \alpha_Y, \sqrt{1-\alpha_X^2-\alpha_Y^2}) \quad \text{with } \alpha_X \text{ and}$$

α_Y being, respectively, the X and Y components of the direction cosines of the unit vector normal to object mirror M_O. Similarly, $\mathbf{n}' = (\alpha'_X, \alpha'_Y, \sqrt{1-\alpha'^2_X-\alpha'^2_Y})$ is the unit vector normal to effective reference mirror M'_R. Under the paraxial approximation and the assumption of small tilts that $\mathbf{n} \approx (\alpha_X, \alpha_Y, 1)$ and $\mathbf{n'} \approx (\alpha_X, \alpha_Y, 1)$, we have from Eq. (1)

$$\delta(x_S, y_S; x, y) \approx \frac{4\pi(d'-d)}{\lambda} - \frac{2\pi(d'-d)}{\lambda f^2}(x_S^2 + y_S^2) + \frac{4\pi}{\lambda f}\left[\left(d'\alpha_X' - d\alpha_X\right)x_S + \left(d'\alpha_Y' - d\alpha_Y\right)y_S\right], \quad (2)$$

Eq. (2) can be rewritten as

$$\delta(x_S, y_S; x, y) \approx \frac{4\pi\Delta(x,y)}{\lambda} - \frac{2\pi\Delta(x,y)}{\lambda f^2}\left[\left(x_S - \bar{x}\right)^2 + \left(y_S - \bar{y}\right)^2\right] + \bar{\phi}, \quad (3)$$

where

$$\Delta(x,y) = d'(x,y) - d(x,y), \qquad \bar{x} = \frac{f(\alpha'_X d' - \alpha_X d)}{d'-d}, \qquad \bar{y} = \frac{f(\alpha'_Y d' - \alpha_Y d)}{d'-d},$$

$$\bar{\phi} = \frac{2\pi\Delta}{\lambda f^2}\left(\bar{x}^2 + \bar{y}^2\right) \quad . \tag{4}$$

Apart from a constant factor, the intensity as the result of interference between these two rays at point A is given by

$$\hat{I}(x,y; x_S, y_S) = I_S(x_S, y_S)\left[1 + \cos\left\{\frac{4\pi\Delta(x,y)}{\lambda} - \frac{2\pi\Delta(x,y)}{\lambda f^2}\left[\left(x_S - \bar{x}\right)^2 + \left(y_S - \bar{y}\right)^2\right] + \bar{\phi}\right\}\right], \quad (5)$$

where $I_S(x_S, y_S)$ is the intensity of the spatially incoherent light source S at point (x_S, y_S). Because each point source is completely incoherent to any other points on the source, the overall intensity on the image sensor is given by:

$$I(x,y) = \iint I_S(x_S, y_S)\left[1 + \cos\left\{\frac{4\pi\Delta(x,y)}{\lambda} - \frac{2\pi\Delta(x,y)}{\lambda f^2}\left[\left(x_S - \bar{x}\right)^2 + \left(y_S - \bar{y}\right)^2\right] + \bar{\phi}\right\}\right]dx_S dy_S, \quad (6)$$

where integration is to be performed over the area of the extended source. After some straightforward algebra, the intensity distribution given by Eq. (6) becomes

$$I(x,y) = B\left\{1 + \left|\mu\left[d(x,y), d'(x,y); \alpha_X, \alpha_Y; \alpha'_X, \alpha'_Y\right]\right|\cos\left[\frac{4\pi\Delta(x,y)}{\lambda} + \phi\right]\right\}, \quad (7)$$

where $B = \iint I_S(x_S, y_S)dx_S dy_S$, and ϕ is the initial phase of the fringe pattern given below. The function $\mu(d(x,y), d'(x,y); \alpha_X, \alpha_Y; \alpha'_X, \alpha'_Y)$ is the longitudinal complex degree of coherence given by

$$\mu[d(x,y), d'(x,y); \alpha_X, \alpha_Y; \alpha'_X, \alpha'_Y] = |\mu|\exp(j\varphi)$$

$$= \frac{\iint I_S(x_S, y_S)\exp\left\{-j\frac{2\pi\Delta(x,y)}{\lambda f^2}\left[(x_S - \bar{x})^2 + (y_S - \bar{y})^2\right]\right\}dx_S dy_S}{\iint I_S(x_S, y_S)dx_S dy_S}, \quad (8)$$

and $\phi = \bar{\phi} + \varphi$. The cosine function in Eq. (7) gives the intensity distribution of the fringe pattern at the observation point A. Eq. (8) looks similar in forms to the corresponding equations in previous papers[3, 6-7], but Eq. (8) is more general as it allow the observation point A to be chosen at an arbitrary position in the interferometer. This generalization can reveal the importance of the role played by the observation lens L2, which has not been made clear in any of the previous papers[3, 6-7].

Now the problem is to find a real and nonnegative light source distribution $I_S(x_S, y_S)$ that maximizes modulus of the

complex degree of coherence at a given observation point A for the specified distances d and d', tilts (α_X, α_Y) and (α'_X, α'_Y). We choose the intensity distribution of a light source of the form

$$I_S(x_S, y_S) = \frac{1}{2}\left[1 + \cos\{-2\pi\gamma[(x_S - \xi_X)^2 + (y_S - \xi_Y)^2] + \beta\}\right], \qquad (9)$$

where the coefficient of $1/2$ is normalization factor, β is the initial phase of FZP, γ is the scaling parameter that determines the focal length of FZP, and ξ_X and ξ_Y are the coordinates of the center of FZP. Comparing FZP source distribution with the corresponding part of complex exponential fringe term in Eq. (8), we find that the modulus of the complex degree of coherence is maximized when we chose the scaling parameter of zone plate source as $\gamma = \pm\Delta/\lambda f^2$ and the center of FZP as $\xi_X = \bar{x} = f(\alpha'_X d' - \alpha_X d)/(d' - d)$, $\xi_Y = \bar{y} = f(\alpha'_Y d' - \alpha_Y d)/(d' - d)$. From the analysis above, we can draw our conclusion that, to produce the coherence function $\mu(d(x, y), d'(x, y); \alpha_X, \alpha_Y, \alpha'_X, \alpha'_Y)$ with a high coherence peak, the scaling parameter γ and shifting parameters ξ_X and ξ_Y of FZP source should satisfy the following matching conditions simultaneously:

$$\text{Scaling parameter: } \gamma = \pm\frac{d' - d}{\lambda f^2} = \pm\frac{\Delta}{\lambda f^2}; \qquad (10)$$

$$\text{Shifting parameters: } \xi_X = \bar{x} = f\frac{\alpha'_X d' - \alpha_X d}{d' - d}, \xi_Y = \bar{y} = f\frac{\alpha'_Y d' - \alpha_Y d}{d' - d}. \qquad (11)$$

Based on the general formula that allows the arbitrary choice of the observation point, let us now clarify the role played by the imaging lens L_2. It is of interest to note a special case. If we focus the imaging lens L_2 on the object mirror, such that the observation point A is placed on the object mirror with $d = 0$, then we find from Eq. (4) and Eq. (8) that $\bar{x} = f\alpha'_X$ and $\bar{y} = f\alpha'_Y$, so that the coherence function becomes insensitive to the local tilts (α_X, α_Y) (or surface inclinations) introduced around the observation point A on the object mirror. Since a rough surface can be interpreted as composition of many microscopic facets with various surface inclinations, this suggests the possibility of a new mode of operation, in which an object with rough (rather than a mirror) surfaces is detected by focusing the imaging lens L_2 exactly at a probing point on the object surface.

Now let us discuss the role of the initial phase β in Eq. (9). If one compares the form of the light source distribution $I_S(x_S, y_S)$ with that of the fringe term in Eq. (5), one can find the perfect similarity between their function forms. This means that these two functions $I_S(x_S, y_S)$ and the fringe term play the exchangeable role in the evaluation of Eq. (5). Therefore, we can rewrite the longitudinal coherence function to an equivalent form:

$$I(x, y; \alpha_X, \alpha_Y; \alpha'_X, \alpha'_Y) = B'\left\{1 + \left|\mu'\left[d(x, y), d'(x, y); \alpha_X, \alpha_Y; \alpha'_X, \alpha'_Y\right]\right|\cos\left[\beta + \phi'(x, y)\right]\right\}, \qquad (12)$$

where $B' = \iint I_F(x_S, y_S; x, y)dx_S dy_S = \iint\left[1 + \cos\left\{\frac{4\pi\Delta(x, y)}{\lambda} - \frac{2\pi\Delta(x, y)}{\lambda f^2}\left[(x_S - \bar{x})^2 + (y_S - \bar{y})^2\right] + \bar{\phi}\right\}\right]dx_S dy_S$ is

the integration of the virtual light source generated from the fringe term in Eq.(5), and

$$\mu'\left[d(x, y), d'(x, y); \alpha_X, \alpha_Y; \alpha'_X, \alpha'_Y\right]$$
$$= \frac{\iint I_F(x_S, y_S, x, y)\exp\left\{-j2\pi\gamma\left[(x_S - \xi_x)^2 + (y_S - \xi_y)^2\right]\right\}dx_S dy_S}{\iint I_F(x_S, y_S, x, y)dx_S dy_S} \qquad (13)$$

is an alternative expression for the complex degree of coherence based on this virtual light source $I_F(x_S, y_S; x, y)$. In Eq. (12), $\phi'(x, y)$ is the initial phase of this new complex coherence function. It should be noted that $\mu = \mu'$ for the measurement that satisfies the zone-plate matching conditions. Because the cosine function of the interference fringe pattern in Eq. (12) includes the initial phase of β, one can perform the phase shift simply by changing the initial phase of this light source zone plate. This can be done with a spatial light modulator (SLM), and no mechanical movement of optical elements is involved for the phase shift.

2. EXPERIMENTS

The schematic illustration of experimental set-up is shown in Fig. 3. Linearly polarized light from a 10mW He-Ne laser was expanded by expander C and collimated by the collimating lens L_C to illuminate a liquid-crystal-based SLM, which modulates light intensity transmitted by polarizer P1 and analyzer P2 placed immediately in front of and behind the SLM. A computer-generated Fresnel zone plate pattern was displayed on the SLM, and was imaged onto a rotating ground glass GG by a combination of lenses L'p and Lp through pinhole PH, which serves as a spatial filter to smooth out the discrete pixel structure of SLM. The image of the Fresnel zone plate on the rotating ground glass serves as a quasi-monochromatic incoherent light source. The ground glass GG is located on the front focal plane of lens L1 with focal length of 150mm. The light from the zone plate source was collimated by L1 and was introduced into a Michelson interferometer made of prism beam splitter BS, reference mirror M_R, and object mirror M_O. A point A near or on the object mirror is imaged by lens L2 onto the sensor plane of CCD camera. The half wave plate WP immediately behind the laser was used to obtain the appropriate illuminating intensity.
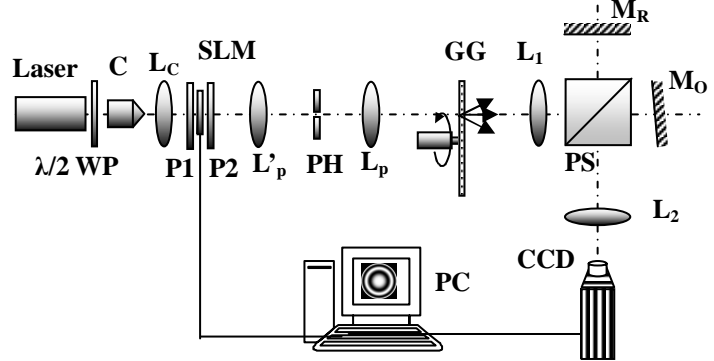
Fig.3. Schematic illustration of experimental setup.

1. 1 Observation condition and degree of coherence

We initialized the distance of two mirrors, M_O and M_R, to be 3mm and set the observation point on the surface of one of the mirrors, say M_O. Then we produced a zone plate source with the scaling parameter $\gamma=\Delta/\lambda f^2$ for Δ=3mm, λ=633nm and f=150mm to satisfy the coherence matching condition by adjusting the zone plate to the proper size, and shifted the center of zone plate to the proper transverse position. To synthesize the coherence degree in a simple way, a small amount of tilt was introduced to M_O. As predicted from Eq. (8), the fringe pattern with high contrast was observed. In the next step, we reset the observation point off the surface of M_O to a certain distance, and then moved this observation point close to the surface of M_O by adjusting the focus of imaging lens L2. It was observed that the visibility of fringes varied with the location of observation point. When the observation point was moved back to the surface of M_O, the fringe contrast became highest. As the observation point was further moved across the location of M_O, the visibility degraded from the peak value to a low level again and did not arise any longer even though the observation point reached the surface of reference mirror M_R. Because the estimated depth of field of our imaging lens L2 is about 1mm, each point on the surface of M_O can be assumed to be well focused

The distance of the observation point from the surface of object mirror (0: surface of M_O; 3: surface of M_R; unit: mm)

Fig. 4. Dependence of coherence degree on the observation condition. (The image of only an area of 200x100 pixels is used for demonstration.)

simultaneously and the coherence distribution along the traverse plane of M_O is so flat that it can be represented by a single average value. The average fringe contrast was obtained by the Fourier transform method. The variation of the average fringe contrast with the observation point is shown in Fig. 4. The abscissa axis indicates the distance of the observation point from the surface of object mirror M_O with its origin on the surface of M_O, and the abscissa value 3.0mm corresponding to the surface of reference mirror M_R. The asymmetry of coherence function can be attributed to the imperfect zone plate matching at initialization, and the aberration of the optical system. The reason why the peak of coherence is beyond the theoretical value 0.5 can be explained by the finite size of zone plate used for the illumination.
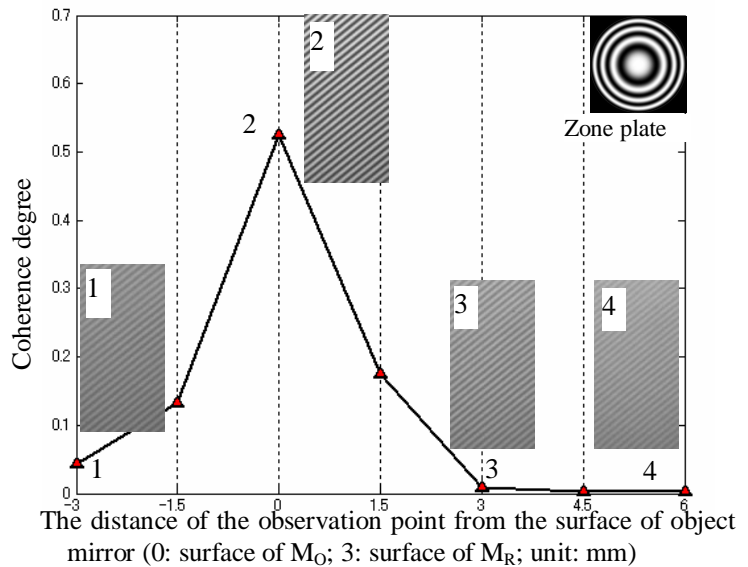
Following the same zone plate initialization process where the focus of the imaging lens L2 was located on the surface of the object mirror M_O, it was observed that the fringes were of high contrast. When we increased the tilt of M_O, the degradation of fringe visibility was not obviously observed, even if the fringe pattern in the view became so dense as to be indiscernible. On the other hand, if we adjusted the focus of lens L2 off the surface of mirror M_O, and increased the tilt of M_O as it had been done above, it was observed that wherever the focus point of lens L2 was located (above or under the surface of M_O), the fringe visibility went down rapidly. The dependence of coherence degree on the tilt is shown in Fig. 5 for different observation points. Thus all the characteristics of the coherence function predicted by our new model have been verified through the experiments. This newly found fact the coherence function is insensitive to the tilt of the focused object opens up a new possibility of profilometry of an object with rough surface. This will be demonstrated through the experiments in the next section.
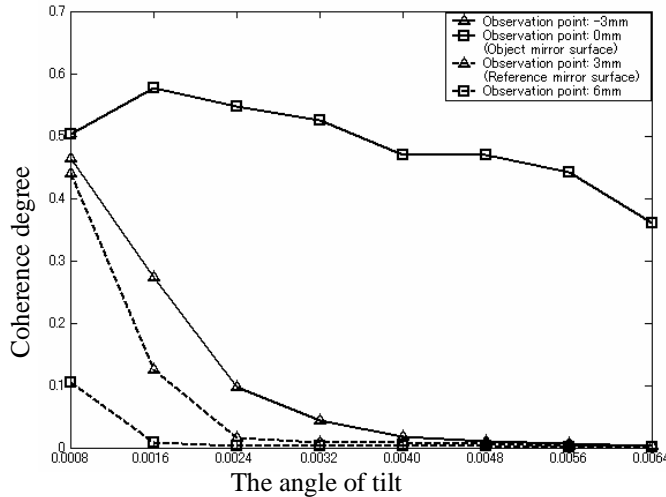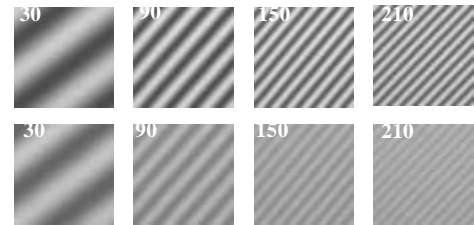

Fig.5 (b) Degradation of fringe visibility with the increment of tilt. On the left-top of the image is the fringe number in the view. Image sequences in the top row and the bottom row were obtained with the observation point on the object surface, and on the reference surface, respectively. (Only a partial area of 50x50 pixels is used for illustration.)

Fig.5 (a) Dependence of coherence degree on the tilt.

1. 2 Profilometry of an object with a rough surface

Before showing the result of profilometry of an object with a rough surface, we briefly explain how to determine the position of the maximum coherence peak. As described in the previous sections, the phase of the fringe pattern can be shifted by scanning the phase of the FZP β_i ($i=1, ..., M$) with SLM (See Eq. (12)). This allows one to determine the fringe contrast at the observation point by the M-step phase-shift technique. It should be noted, however, that the degree of coherence obtained by this FZP-based phase shift technique gives true values only at the coherence maximum where γ of FZP matches the real object height Δ; fortunately this coherence maximum is the location of our interest. If one scans the longitudinal coherence function by changing the FZP parameter γ_i ($i=1, ..., N$) by N steps, the total scanning process requires as many as M×N sets of FZPs, which slows the speed of measurement. If we know the FZP phase value β_1 that gives the maximum fringe intensity at the observation point, the FZP phase value β_2 that gives the intensity minimum the same observation point can be obtained simply by $\beta_2=\beta_1\pm\pi$, and vice verse. In this case, the fringe contrast can be obtained from just two FZPs instead of M. This is in fact possible. If we set a certain value of γ_i ($i=1, ..., N$) for longitudinal coherence scan, then the corresponding height Δ_i ($i=1, ..., N$) can be determined from the matching condition of Eq. (10). From these values, β_{1i} for the maximum value of $I_i(x, y)$ can be easily found out by the straightforward calculations. Then, based on the series of β_{1i} ($i=1, ..., N$) generated from γ_i ($i=1, ..., N$) series, a γ-β_1 look-up table can be created for the FZP series that give the maximum intensity at the observation point. Then, we can obtain β_{12} that gives the intensity minimum, simply by adding $\pm\pi$ to the phase value β_1. The number of FZPs for scanning decreases to 2N. An example of the γ-β_1 look-up table is shown in Table. 1.

Table. 1 Demonstration of γ-β_1 look-up table

γ (λ=633nm, f=150mm)	......	1mm / λf^2	1.01mm / λf^2	......	4mm /λf^2	......
β_1	......	2.7489	5.4978	......	4.7124	......

In the experiment of profilometry, an Aluminum Chinese coin of 2 FEN was used as the sample, and was focused by the imaging lens L2. First we generated FZPs' series with the increasing scaling parameter $\gamma_i \propto 1\sim4$mm (interval: $\delta\gamma_i \propto 10\mu$m) of the specific initial phase β based on the γ-β_1 look-up table. Then, for each value of γ_i used for the longitudinal coherence scan, we calculated the intensity difference using two FZPs with phase β_1 and $\beta_2=\beta_1+\pi$. With the scanning time interval of 120ms (depending on the response speed of SLM), it took $2\times400\times0.12$s=96s to complete the whole scanning process of the longitudinal coherence. Figure 6 (a) shows the change of FZP source shape during the scanning process, and Fig.6 (b) show the variation of the intensity difference as the longitudinal coherence is scanned. The location of the maximum intensity difference indicates the position of the surface to be sensed. Figure 7 (a) shows a coin used as a sample object, whose height distribution obtained by measurement with ~0.5× magnification is shown in Fig. 7(b).
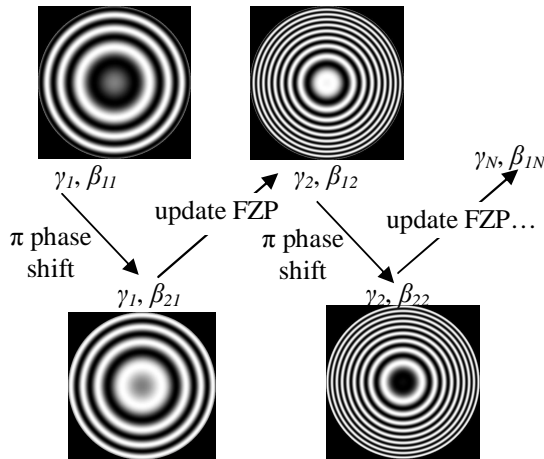

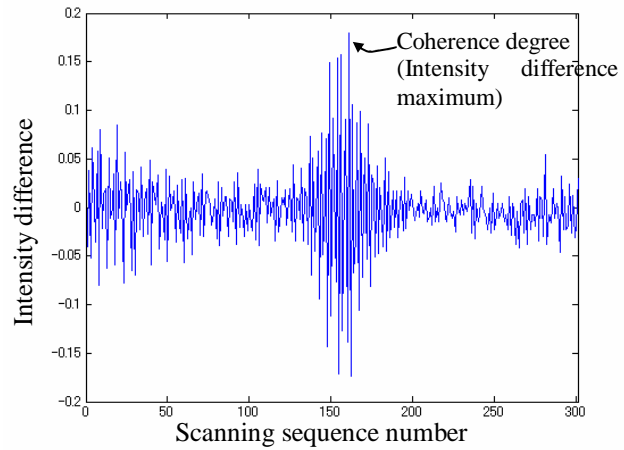Fig. 6 (a) Demonstration of zone plate scanning sequence.

Fig. 6 (b) Intensity difference fluctuation to indicate the local height of an arbitrary observation point on the sample surface.

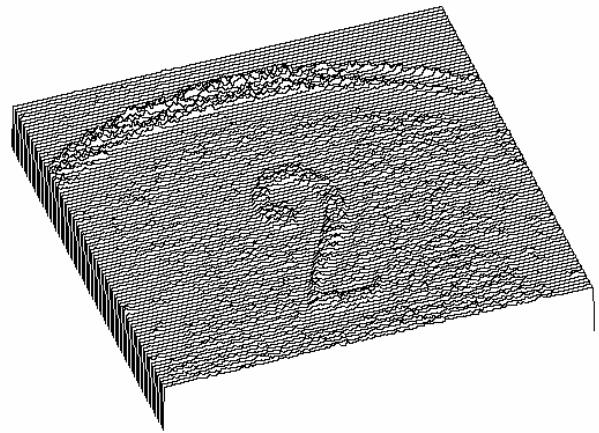Fig. 7 (a) The 2-Fen Chinese coin used as a sample for the profilometry.

Fig. 7 (b) The synthesized surface height of the coin.

3. CONCLUSION

We have presented a generalized theory for interference fringe formation with a synthetic source for spatial coherence control. The relation between the observation point and the coherence function has been clarified in theory and verified by experiments. The potential applications in the profilometry and tomography have been explored through the measurements of an object with rough surfaces. As a means to obtain the coherence peak position quickly, the use of a look-up table for FZP phase parameter has been proposed and applied to profilometry.

REFERENCES

1. See, for example, D. Huang, E. A. Swanson, C. P. Lin, J. S. Schuman, W. G. Stinson, W. Chang, M. R. Hee, T. Flotte, K. Gregory, C. A. Puliafito, J. G. Fujimoto, "Optical coherence tomography," *Science* **254**, 1178-1181, 1991.

2. See, for example, B. S. Lee and T. C. Strand, "Profilometry with a coherence scanning microscope," *Appl. Opt.* **29**, 3784-3788, 1990; T. Dressel, G. Hausler, and H. Venzke, "Three-dimensional sensing of rough surfaces by coherence radar," *Appl. Opt.* **31**, 919-925, 1992; L. Deck, P. de Groot, "High-speed noncontact profiler based on scanning white light interferometry," *Appl. Opt.* **33**, 7334-7338, 1994.

3. J. Rosen and M. Takeda, "Longitudinal spatial coherence applied for surface profilometry," *Appl. Opt.* **39,** 4107-4111, 2000.

4. M. Takeda, J. Rosen, and Z. Duan, "Space-Time analogy in synthetic coherence functions applied to optical tomography and profilometry", *Proc. of ICLAOM-03*, C. Shakher, and D. S. Mehta, 1-8, Anamaya Publisher, New Delhi, India, 2003.

5. Z. Duan, M. Gokhler, J. Rosen, H. Kozaki, N. Ishii, and M. Takeda, "Spatial coherence optical tomography: a new principle for dispersion-free measurement," *Proc.of Asian Symposium on Biomedical Optics and Photomedicine BOPM*, 138-139, Sapporo, Japan, 2002.

6. Z. Duan, M. Gokhler, J. Rosen, H. Kozaki, N. Ishii, and M. Takeda, "Synthetic spatial coherence function for optical tomography and profilometry: simultaneous realization of longitudinal coherence scan and phase shift," *Interferometry XI: Technique and Analysis, Proc. of SPIE*, K. Creath and J. Schmit, 4777, 110-177, Seattle, 2002.

7. M. Gokhler, Z. Duan, J. Rosen, and M. Takeda, "Spatial coherence radar applied for tilted surface profilometry," *Opt. Eng.* **42**(3), 830-836, 2003.

8. W. Wang, H. Kozaki, J. Rosen, and M. Takeda, "Synthesis of longitudinal coherence functions by spatial modulation of an extended light source: a new interpretation and experimental verifications," *Appl. Opt.* **41**, No.10, 1962-1971, 2002.

9. V. P. Ryabukho, D. V. Lyakin, and M. I. Lobachev, "The effects of temporal and longitudinal spatial coherence in a disbalanced-arm Interferometer," *Tech. Phys. Lett.*, **30**, No. 1, 64–67, 2004.

10. V. Ryabukho, D. Lyakin, and M. Lobachev, "Influence of longitudinal spatial coherence on the signal of a scanning interferometer, *Opt. Lett.*, **29**, No. 7, 2004 (to appear).